

# Flow and instability of thin films on a cylinder and sphere

DAISUKE TAKAGI AND HERBERT E. HUPPERT†

Institute of Theoretical Geophysics, Department of Applied Mathematics and Theoretical Physics,  
University of Cambridge, Wilberforce Road, Cambridge CB3 0WA, UK

(Received 15 June 2009; revised 3 December 2009; accepted 3 December 2009)

We investigate the dynamics of thin films driven by gravity on the outer surface of a cylinder and sphere. The surface is rigid, stationary and the axis of the cylinder is horizontal. An instantaneous release of a constant volume of fluid at the top of the cylinder or sphere results initially in a two-dimensional or axisymmetric current respectively. The resultant flow of a thin film of fluid is described using lubrication theory when gravity and viscous forces govern the dynamics. We show that the thickness of the flow remains uniform in space and decreases in time like  $t^{-1/2}$  near the top of both the cylinder and the sphere. Analytic solutions for the extent of the flow agree well with our experiments until the advancing front splits into a series of rivulets. We discuss scalings of the flow at the onset of the instability as a function of the Bond number, which characterizes the relative importance of gravity and surface tension. The experiments, conducted within an intermediate range of Bond numbers, suggest that the advancing front becomes unstable after it has propagated a critical distance, which depends primarily and monotonically on the volume of fluid and not on the viscosity of fluid. Releasing a sufficiently large volume of fluid ensures that rivulets do not develop on either a cylinder or sphere.

---

## 1. Introduction

Many problems in industrial and natural settings involve the flow of thin liquid films, some of which are driven by gravity on a rigid surface (Oron, Davis & Bankoff 1997). These include the application of coatings on manufactured products and the spreading of sauce on food. A naturally occurring example is the flow of water on stalactites that hang from the ceilings of limestone caves (Short *et al.* 2005). At larger scales, the ascent of buoyant magma below solid rocks and the spreading of lava on volcanoes are further examples of geological problems. The recurring feature in all these examples is that fluid is in contact with, and driven along, a rigid boundary due to the action of gravity. Effects due to inertia are negligible in the bulk region of the flow, where gravity and viscous forces dominate.

The flow of driven thin films has received considerable attention within the scientific community largely because the leading edge of the flow gives rise to the fascinating phenomenon of a fingering instability. Laboratory experiments have shown that a thin film of Newtonian fluid flowing down an inclined plane can become unstable at the front and split into a series of rivulets (Huppert 1982; Silvi & Dussan 1985). Rivulets develop in a similar manner when a thin film is driven by a centrifugal force (Melo,

† Email address for correspondence: heh1@esc.cam.ac.uk

Joanny & Fauve 1989; Fraysse & Homsy 1994; Wang & Chou 2001) or by a spatial gradient in surface tension (Cazabat *et al.* 1990). The instability has been studied by incorporating effects because of surface tension in a small region near the advancing front of the flow, where a capillary ridge develops before splitting into rivulets (Troian *et al.* 1989; Goodwin & Homsy 1991). A crossflow perturbation of the flow front develops thicker regions that advance more rapidly, a possible mechanism of the fingering instability (Spaid & Homsy 1996). Macroscopic perturbations can be caused by microscopic corrugations in the contact line (Bertozi & Brenner 1997), suggesting that minor variations in topography, in addition to thermal effects, may influence the development of candle wax drips and branches of lava flows on volcanoes.

We extend previous studies of thin films to consider driven films featuring a moving contact line on curved surfaces. Lubrication theory has been applied to describe thin films flowing in between curved gaps (Stone 2005) and on curved substrates with a free surface (Roy, Roberts & Simpson 2002). It is fruitful to assess the applicability of the theory to thin films featuring a moving contact line (Davis 1983), which may not influence the bulk flow. Thin films on the outer surface of a cylinder and sphere are considered as two special cases where the slope of the substrate changes slowly in the direction of flow. Thin films flowing on the inner surface of a cylinder and sphere are also worth considering and will be addressed in a future publication. The theory is based on the following three conditions. First, the front of the flow is assumed to have extended a distance much longer than the characteristic film thickness. Second, the component of gravity is approximated to increase linearly in the flow direction, which holds near the top of the cylinder and sphere. Third, surface tension is considered to be negligible everywhere except possibly near the leading front of the flow. We examine the effect of a curved substrate on the flow and its possible instability of thin films in two specific cases.

In the first case, we consider the instantaneous release of a constant volume of viscous fluid from a line source at the top of a cylinder. We stress that the cylinder does not rotate about its horizontal axis. The resultant flow is initially two-dimensional; an analytic solution describing its form and extent is obtained in §2 using lubrication theory. Related problems that have been investigated theoretically include thin films on a rotating cylinder (Moffatt 1977) and steady rivulet flows on a stationary cylinder (Duffy & Moffatt 1995). We note that once the rotation of the cylinder, or the supply of fluid, has stopped, the structure of the flow is expected to tend to a long time limit, which is closely related to what we consider here.

In the second case, we consider the instantaneous release of a constant volume of viscous fluid from a point source at the top of a sphere. The initial spreading of fluid near the source is the axisymmetric counterpart of the two-dimensional flow in our first case. The problem on the sphere falls in the same category of axisymmetric spreading as flow from the top of a cone, which is presented as mathematical exercise 7.12 in the introductory textbook by Acheson (1990). In §3, we develop theoretical results and show that the spreading on a stationary sphere is closely related to spin coating, where a drop of fluid spreads and develops a fingering instability on a rotating plane (Melo *et al.* 1989; Fraysse & Homsy 1994; Wang & Chou 2001). Consequently, the spreading on a sphere is expected to develop a fingering instability at the leading edge in a similar manner to a spinning drop.

In §4, corresponding experiments are reported and shown to agree well with our theoretical predictions until the advancing front splits into a series of rivulets. The rivulets continue to extend until they eventually detach, before they have reached

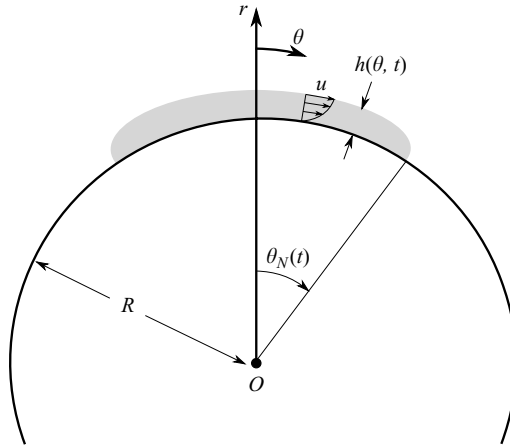


FIGURE 1. Sketch of a thin film driven by gravity at the top of a cylinder. Flow is denoted to have thickness  $h(\theta, t)$  and extends an arclength  $R\theta_N(t)$  from the vertical line of symmetry.

the bottom of the cylinder or sphere. The detachment of fluid from the underside of the cylinder and sphere is similar to that from the underside of an inclined plane (Rothrock 1968; Indeikina, Veretennikov & Chang 1997). We note that the development of rivulets at the flow front and the detachment of fluid before reaching the bottom prevent the fluid from completely coating the cylinder or sphere.

Finally, in § 5, the fingering instability at the leading front of the flow is discussed. A scaling analysis of the governing equations suggests that the non-dimensional flow length at the onset of the instability depends on the Bond number of the flow. The ideas are partly based on the scalings obtained previously for flow down an inclined plane at a small Bond number (Troian *et al.* 1989; Goodwin & Homsy 1991). We obtain approximate conditions at the onset of a fingering instability on a cylinder and sphere in the two limits of small and large Bond numbers. The results suggest that rivulets do not develop on a cylinder or sphere when a sufficiently large volume of fluid is released.

## 2. Two-dimensional flow on a cylinder

A theoretical framework for describing flow on the outer surface of a cylinder of radius  $R$  is developed in polar coordinates  $(r, \theta)$ , where  $r = R$  represents the surface and the azimuth angle  $\theta$  is measured from the vertical as in figure 1. We consider the instantaneous release of a constant volume of viscous fluid from a line source at the top of the cylinder such that the resultant flow is initially two-dimensional, independent of the direction normal to the  $(r, \theta)$  plane. By the vertical line of symmetry, we restrict attention to flow on the right half of the cylinder. A constant cross-sectional area  $A$  of fluid is considered to have depth  $h(\theta, t)$  and extend an arclength  $R\theta_N(t)$  along the surface of the cylinder from the vertical as shown in figure 1.

A long wave approximation is adopted, provided that the fluid depth is much smaller than its extent:

$$h \ll R\theta_N. \quad (2.1)$$

The approximation is expected to hold soon after the fluid is released on a cylinder of sufficiently large radius  $R$ . Because flow is predominantly tangential to the surface

of the cylinder, the pressure in the fluid is given by

$$p = p_0 + \rho g(R + h - r) \cos \theta - (\gamma/r^2) \partial^2 h / \partial \theta^2, \quad (2.2)$$

where  $\rho$  is the density of fluid,  $g$  is the gravity,  $p_0$  is the atmospheric pressure and  $\gamma$  is the surface tension. The  $\theta$  component of the momentum equation is given by

$$\nu \partial^2 u / \partial r^2 = (1/\rho r) \partial p / \partial \theta - g \sin \theta, \quad (2.3)$$

where  $\nu$  is the kinematic viscosity of the fluid and  $u$  is the  $\theta$  component of the flow velocity. The pressure given by (2.2) remains approximately uniform in the bulk region of the flow given the following two conditions. First, the depth of fluid must vary slowly along the substrate and satisfy

$$\partial h / \partial \theta \ll R \tan \theta. \quad (2.4)$$

Condition (2.4) is expected to hold everywhere except possibly near the flow front and ensures that contribution to (2.3) from the  $\rho g(R + h - r) \cos \theta$  term on the right-hand side of (2.2) is negligible. Second, effects due to surface tension must be small everywhere except possibly near the flow front, requiring that the final term of (2.2) does not play a role in the equation of motion given by (2.3). By comparing the magnitude of the first and second terms on the right-hand side of (2.3), we obtain the corresponding condition

$$\gamma \partial^3 h / \partial \theta^3 \ll \rho g R^3 \sin \theta. \quad (2.5)$$

Importantly, we note that the bulk structure of the flow is relatively unaffected by the specific dynamics of the small region near the flow front (Huppert 1982; Troian *et al.* 1989). Under these conditions, the bulk region of the flow is governed primarily by viscous forces and the component of gravity along the flow. The solution satisfying (2.3) with the first term on the right-hand side neglected, along with the no-slip condition on the rigid surface and vanishing tangential stress on the free surface, is given by

$$u = \frac{1}{2} y (2h - y) g \sin \theta / \nu, \quad (2.6)$$

where  $y = r - R$  is the radial coordinate measured from the surface of the cylinder. The velocity profile is parabolic in  $y$  and identical to that arising on an inclined plane with a constant slope  $\theta$  to the horizontal (Huppert 1982). The local flow on a sufficiently large cylinder does not experience the curvature in the substrate. The depth-integrated velocity of the flow,

$$Q = \int_0^h u \, dy, \quad (2.7)$$

does not depend on the curvature of the substrate  $R$ .

The governing equations for the unknown free surface  $h(\theta, t)$  are formulated by conserving the mass of fluid, both locally and globally. Substituting (2.6) into (2.7) followed by the local conservation of mass in cylindrical polar coordinates,  $\partial h / \partial t + R^{-1} \partial Q / \partial \theta = 0$ , we obtain

$$\frac{\partial h}{\partial t} + \frac{g}{3\nu R} \frac{\partial}{\partial \theta} (\sin \theta h^3) = 0. \quad (2.8)$$

The total cross-sectional area of fluid is independent of time and is expressed as

$$A = R \int_0^{\theta_N(t)} h(\theta, t) \, d\theta, \quad (2.9)$$

which ensures that mass is conserved globally. This completes the formulation of the problem.

The length and time scales of the flow initially near the top of the cylinder can be determined by considering the scaling factors of the governing equations (2.8) and (2.9). For small  $\theta$  such that  $\sin \theta \approx \theta$  to leading order, the two terms in (2.8) scale as  $h/t$  and  $gh^3/\nu R$ , respectively. Meanwhile, (2.9) indicates that  $A \sim hx$ , where  $x = R\theta$  is a characteristic length of the current. The only dimensional groups appearing in the governing equations for  $h$  in terms of  $x$  and  $t$  are therefore  $g/\nu R$  and  $A$ . The equations can be non-dimensionalized by scaling all lengths by

$$L \equiv A^{1/2} \tag{2.10}$$

and time by

$$T \equiv \nu R/gA. \tag{2.11}$$

The radius of the cylinder,  $R$ , only appears in the time scale and not in the length scale of the bulk flow.

The system of (2.8) and (2.9) is solved near the top region of the cylinder, where  $\theta \ll 1$ , as follows. Given that the characteristic length and time scales are given by (2.10) and (2.11), respectively, it is natural to seek solutions to (2.8) with  $\sin \theta \approx \theta$  of the form

$$h = A^{1/2} f(t/T). \tag{2.12}$$

The function  $f$  to be determined is independent of  $\theta$  because  $\theta$  does not appear in the scalings of the two terms in (2.8) when  $\sin \theta \approx \theta$ . By substituting (2.12) into (2.8), we obtain  $f' + f^3/3 = 0$ , which can be immediately integrated to give

$$f(s) = [3(s + c)/2]^{-1/2} \tag{2.13}$$

for some constant  $c$ . If the fluid has uniform thickness  $h_0$  initially when it is released at time  $t = 0$ , then the starting time is offset by  $c = 2(A^{1/2}/h_0)^2/3$  for the similarity form (2.12) to satisfy the initial condition. However, the required offset  $c$  is negligible when the initial thickness is not too small,  $h_0 > A^{1/2}$ , or equivalently when the flow front is close to the top of the cylinder at the time of release of fluid, as was the case in all our experiments. At large times,  $t \gg cT$ , the solution (2.13) in dimensional form reduces to

$$h(t) = \left( \frac{3R\nu}{2g} \right)^{1/2} t^{-1/2}, \tag{2.14}$$

which indicates that the thickness is independent of  $\theta$  and decreases with time like  $t^{-1/2}$ . The subsequent term of order  $\epsilon$  in the expansion about the leading-order solution (2.14), where  $\theta = O(\epsilon)$ , is also independent of the spatial coordinate. The solution (2.14) is independent of  $\theta$  to order  $\epsilon^2$  because of the symmetry of the problem.

We note that the solution of uniform film thickness is related to the boundary-layer thickness of a stagnation-point flow towards a flat boundary (Acheson 1990). Both gravity-driven flow near the top of a cylinder and two-dimensional straining flow along the flat boundary increase linearly with distance. It follows by mass conservation that in both cases the thickness of the flow is uniform along the boundary.

The length of the current is obtained by imposing the condition that the total cross-sectional area of fluid is conserved and given by (2.9). By substituting (2.14) into (2.9) and rearranging, we determine the length of the current

$$R\theta_N(t) = \left( \frac{A^2 g}{6R\nu} \right)^{1/2} t^{1/2}. \tag{2.15}$$

We note that the dependence on the amount of fluid released,  $A$ , only appears in the expression for the length and not in the expression for the depth of the flow. The flow near the top of the cylinder takes a similarity form and is independent of the initial conditions. By substituting solutions (2.13) and (2.15) into conditions (2.1) and  $\theta_N \ll 1$ , we determine that the solution for the flow length given by (2.15) is valid for

$$1 \ll t/T \ll R^2/A. \quad (2.16)$$

The first condition,  $t \gg T$ , ensures that the thickness of the current is small compared to its length. The second condition,  $t/T \ll R^2/A$ , arises because the solution given by (2.14) is limited to the region near the top of the cylinder.

We now discuss the small region at the flow front, which we have neglected so far. By eliminating time from solutions (2.14) and (2.15), we determine that the flow has a sharp leading front of thickness

$$h_N = A/R\theta_N. \quad (2.17)$$

The unphysically sharp front is expected to be resolved by a thin boundary layer with length scale  $l \ll R\theta_N$ , which is small under the following conditions. When effects due to surface tension are neglected, lubrication theory breaks down near the front of the current (Goodwin & Homsy 1991). The velocity normal to the substrate is no longer small in the region at the flow front. In that case, the length of the boundary layer at the front of the current is expected to scale like  $l \sim h_N$ , which is always smaller than the bulk flow by condition (2.1).

When surface tension plays a role, in addition to viscous forces and gravity, the left- and right-hand sides of (2.5) are of the same order of magnitude in the region near the flow front. By considering the scaling factors of (2.5), we obtain  $l \sim (\gamma h_N / \rho g \sin \theta_N)^{1/3}$ , which is consistent with the corresponding scaling for the length scale of the tip of the current down an inclined plane (Huppert 1982; Troian *et al.* 1989). This can be written as

$$l \sim h_N (Ca)^{-1/3}, \quad (2.18)$$

where  $Ca$  is a capillary number of the flow in the region near the front given by

$$Ca \equiv \rho g \theta_N h_N^2 / \gamma. \quad (2.19)$$

The capillary number measures the relative importance of viscous forces, which are exactly balanced by gravity, compared to surface tension near the flow front. By substituting (2.15) and (2.17) into (2.19), we determine that the capillary number evolves like  $t^{-1/2}$ . Instead of working with the capillary number, it is convenient to introduce a Bond number defined as

$$Bo \equiv \rho g A^{3/2} / \gamma R, \quad (2.20)$$

which is expressed in terms of input parameters that do not vary in time. By setting  $l$  in (2.18) to be much smaller than  $R\theta_N$  and eliminating  $h_N$  using (2.17), we determine that the region of the flow front influenced by surface tension remains small compared to the bulk flow as long as

$$\theta_N \gg Bo^{-1/5} A^{1/2} / R. \quad (2.21)$$

Equivalently, by substituting (2.15) into (2.21), we obtain

$$t \gg Bo^{-2/5} T \quad (2.22)$$

as the condition when surface tension plays a negligible role in the bulk region of the flow.

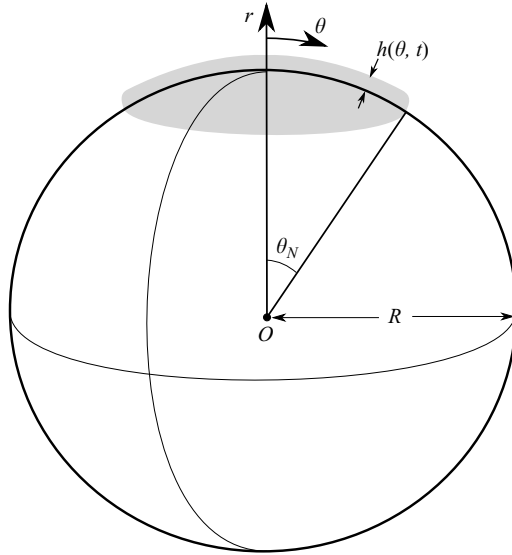


FIGURE 2. Sketch of a thin film of fluid spreading axisymmetrically at the top of a sphere.

In summary, the bulk structure of the flow has uniform thickness given by (2.14) behind an advancing front given by (2.15). The prediction for the flow length is given by (2.15) provided that conditions (2.16) and (2.22) hold. We now present corresponding results for the axisymmetric spreading of fluid at the top of a sphere, before comparing our theoretical predictions with data from laboratory experiments.

### 3. Axisymmetric flow on a sphere

The methods presented in §2 for the two-dimensional flow around a cylinder can be readily applied to the axisymmetric flow on a sphere. Consider the outer surface of a rigid sphere represented by  $r = R$  in spherical polar coordinates, where  $\theta$  is the usual zenith angle from the vertical axis. A constant volume  $V$  of viscous fluid is released instantaneously at the top point of the sphere such that the resultant flow is initially axisymmetric as sketched in figure 2. When the extent of the flow, denoted by  $R\theta_N(t)$ , is much greater than the film thickness denoted by  $h(\theta, t)$ , the flow velocity  $u(r, \theta, t)$  is predominantly along the surface of the sphere, in the  $\theta$  direction. Assuming that conditions (2.1), (2.4) and (2.5) hold in the bulk region of the flow as in §2, and using lubrication theory as before, we obtain the same velocity profile as for viscous spreading on a cylinder. Thus, the depth-integrated velocity is again given by

$$Q = \frac{1}{3}g \sin \theta h^3/\nu. \tag{3.1}$$

Substituting (3.1) into the local mass conservation in spherical polar coordinates given by  $\partial h/\partial t + (R \sin \theta)^{-1} \partial(\sin \theta Q)/\partial \theta = 0$ , we obtain

$$\frac{\partial h}{\partial t} + \frac{g}{3\nu R \sin \theta} \frac{\partial}{\partial \theta} (\sin^2 \theta h^3) = 0. \tag{3.2}$$

The total volume of fluid is independent of time and expressed as

$$V = 2\pi R^2 \int_0^{\theta_N(t)} h \sin \theta \, d\theta. \tag{3.3}$$

The governing equations given by (3.2) with  $\sin\theta \approx \theta$  and (3.3) can be non-dimensionalized by scaling all lengths by

$$L_V \equiv V^{1/3} \quad (3.4)$$

and time by

$$T_V \equiv \nu R/gV^{2/3}. \quad (3.5)$$

The curvature of the substrate only appears in the time scale and not in the length scale of the flow, just like the flow on a cylinder in §2.

The system of (3.2) and (3.3) is solved in the region at the top of the sphere, where  $\theta \ll 1$ , using the same methods as before, to obtain

$$h(t) = \left( \frac{3R\nu}{4g} \right)^{1/2} t^{-1/2}. \quad (3.6)$$

The solution given by (3.6) indicates that the thickness of the bulk structure remains uniform near the top of the sphere. Note that the thickness of fluid on a sphere of radius  $R$  given by (3.6) is identical to the thickness of fluid on a cylinder of radius  $R/2$ , as can be verified using (2.14). The expression (3.6) is also identical to the thickness of a constant volume  $V$  of fluid rotated at angular velocity  $\omega$  about its centre of mass on a plane, where  $\omega^2 = g/R$  (Melo *et al.* 1989). The mathematical reason is that the governing equations for fluid spreading near the top of a sphere, (3.2) and (3.3), where  $\sin\theta \approx \theta$  and  $g/R = \omega^2$ , reduce to corresponding equations for a spinning volume of fluid. Physically, fluids spreading both on the top of a stationary sphere and on the rotating plane experience a body force, which increases linearly with distance away from the point of release. The body force is gravity on the sphere or centrifugal on the rotating plane.

By substituting (3.6) into (3.3), we determine that the length of the current is given by

$$R\theta_N(t) = \left( \frac{4V^2g}{3\pi^2R\nu} \right)^{1/4} t^{1/4}. \quad (3.7)$$

The radius of the leading edge of the flow increases like  $t^{1/4}$  as long as effects on the bulk flow due to surface tension are small.

An analysis similar to the previous one indicates that the capillary region, where capillary forces are important near the flow front, is small compared to the bulk flow provided that

$$\theta_N \gg Bo_V^{-1/6} V^{1/3}/R, \quad (3.8)$$

where  $Bo_V$  is a Bond number defined as

$$Bo_V \equiv \rho g V / \gamma R. \quad (3.9)$$

The capillary region becomes relatively small after the flow front has extended sufficiently far. By substituting (3.7) into (3.8), we determine that surface tension plays a negligible role in the bulk region of the flow when

$$t \gg Bo_V^{-2/3} T_V. \quad (3.10)$$

The regime of validity of solutions (3.6) and (3.7) is further constrained by

$$1 \ll t/T_V \ll R^4/V^{4/3}, \quad (3.11)$$

which can be investigated experimentally by releasing fluid on a sphere of sufficiently large radius  $R$ . The volume of fluid must be sufficiently large that the Bond number

is not too small to satisfy (3.10) and sufficiently small that it spreads as a thin film near the top of the sphere to satisfy (3.11).

#### 4. Experiments

The theoretical predictions derived in §§2 and 3 were tested against a suite of laboratory experiments. In particular, (2.15) and (3.7) were compared with flow lengths on a cylinder and sphere, respectively. Experimental set-ups and results are presented first for flows on a cylinder followed by flows on a sphere.

##### 4.1. Flow on a perspex cylinder

A perspex cylinder of radius 15.0 cm and width 11.0 cm was fixed between two parallel and vertical plates, perpendicular to the axis of the cylinder. The cylinder resembled the structure of a wheel, fixed and confined laterally by sidewalls. At the top of the cylinder, a constant volume of either pure glycerine or golden syrup was held behind a removable lock gate, 2.0 cm away from a rigid and vertical wall. Flow down the outer surface of the cylinder was initiated by a near-instantaneous lift of the gate.

A standard digital camera pointed in the direction parallel to the axis of the cylinder and recorded images of the resultant flow at 15 frames per second. The flow was observed both directly from its side and in plan form through a mirror as shown in the images of figure 3. The flow near the sidewalls was observed to shear laterally with the leading edge of the flow deforming accordingly. This is possibly due to contact line pinning on the sides and the curvature of the substrate, which allows fluid further along the flow to be driven by a larger body force. However, the central region of the flow appeared to be two-dimensional and unaffected by the sidewalls, as indicated by a flat leading front in figure 3(b). The flow front, after advancing some distance, split into a pair of rivulets. The rivulets continued to flow as shown in figure 3(c) until they reached some extent on the underside of the cylinder, where they dropped as viscous threads (figure 3e). The point of detachment advanced approximately 5 cm further along the underside of the cylinder and appeared to remain stationary thereafter.

The viscosity and volume of the released fluid were varied in a series of experiments on the cylinder. Representative values of the kinematic viscosity of golden syrup and glycerine were taken to be  $\nu = 4.5 \times 10^2 \text{ cm}^2 \text{ s}^{-1}$  and  $\nu = 5.1 \text{ cm}^2 \text{ s}^{-1}$ , respectively, based on measurements using U-tube viscometers. Although the viscosity of fluid may have fluctuated slightly as a result of minor temperature variations in the laboratory, the flow lengths recorded in every experimental run are relatively insensitive to minor variations in viscosity. The flow length on a cylinder or sphere scales like  $\nu^{-1/2}$  in (2.15) or  $\nu^{-1/4}$  in (3.7), respectively.

Figure 4 shows a plot of non-dimensional flow extents against non-dimensional time on logarithmic scales for different experiments on the cylinder. The data for the initial flow extending with a single front collapse onto the theoretical curve given by (2.15). Minor discrepancies between the theory and experiments conducted by releasing a cross-sectional area  $A = 10.5 \text{ cm}^2$  of golden syrup and  $A = 5.2 \text{ cm}^2$  of glycerine are attributed to the shear stress on the sidewalls, which may have retarded the flow. Experiments conducted by releasing  $A = 4.2 \text{ cm}^2$  and  $A = 6.3 \text{ cm}^3$  of golden syrup are in excellent agreement with the theoretical predictions until the front of the flow split into a pair of rivulets. Once the front developed a fingering instability, the subsequent leading fronts extended further along the cylinder than predicted by (2.15).



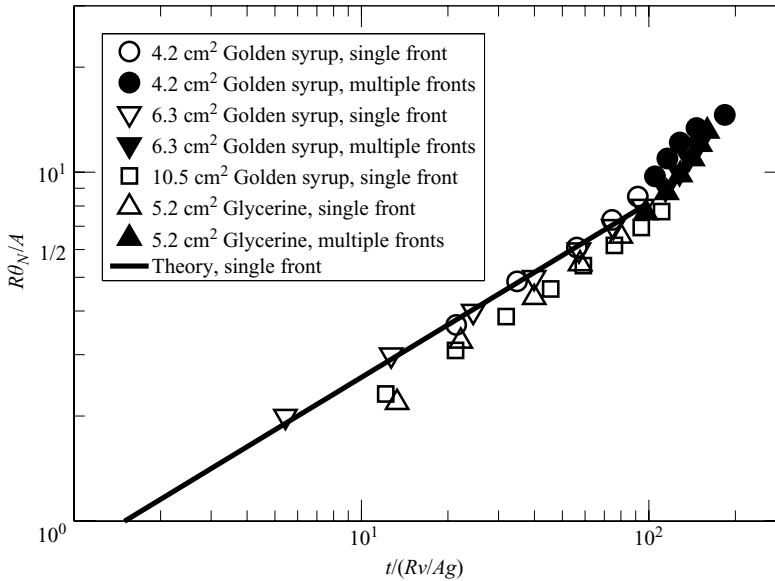


FIGURE 4. Plot of non-dimensional flow extents on a cylinder against non-dimensional time using logarithmic axes. Different symbols correspond to different experiments. The symbols are either open or closed, with the latter indicating that rivulets have developed at the front of the flow. The black line is the theoretical relationship given by (2.15).

#### 4.2. Flow on a vinyl beach ball

Experiments were conducted to investigate viscous flow on a sphere. A vinyl beach ball of radius  $23.5 \pm 0.5$  cm was secured at its base. The surface of the beach ball was reasonably spherical and rigid. A cylindrical lock was positioned carefully at the top of the beach ball using a spirit level such that its axis pointed vertically. A constant volume of golden syrup was poured inside the lock, which could be swiftly raised by guiding it along a vertical rail to release the syrup. The radius of the gate was either 2 cm or 5 cm and made little difference to the resultant flow.

The near-instantaneous release of golden syrup resulted initially in an axisymmetric current from the top of the sphere as shown in figure 5(b). The structure of the flow extended with a circular plan form and then slowly started to deform in shape (figure 5c). Modulations then developed at the leading edge of the flow, as shown in figure 5(d). Soon after, a series of rivulets developed at the front (figure 5e). The rivulets are similar to those produced at the front of an initially axisymmetric spreading on a rotating plane (Melo *et al.* 1989; Fraysse & Homay 1994). The rivulets continued to flow down the sphere until they reached some extent on its underside, where they detached and dropped in the form of threads.

The flow lengths along six representative directions were recorded at different intervals. Figure 6 shows that the mean flow lengths agree well with the theoretical curve before the leading edge of the flow developed a fingering instability. We now discuss scaling laws of the flow at the onset of the instability.

## 5. Discussion

It is widely accepted that a capillary ridge near the flow front plays an important role at the onset of the instability. Numerous other possible factors are believed to

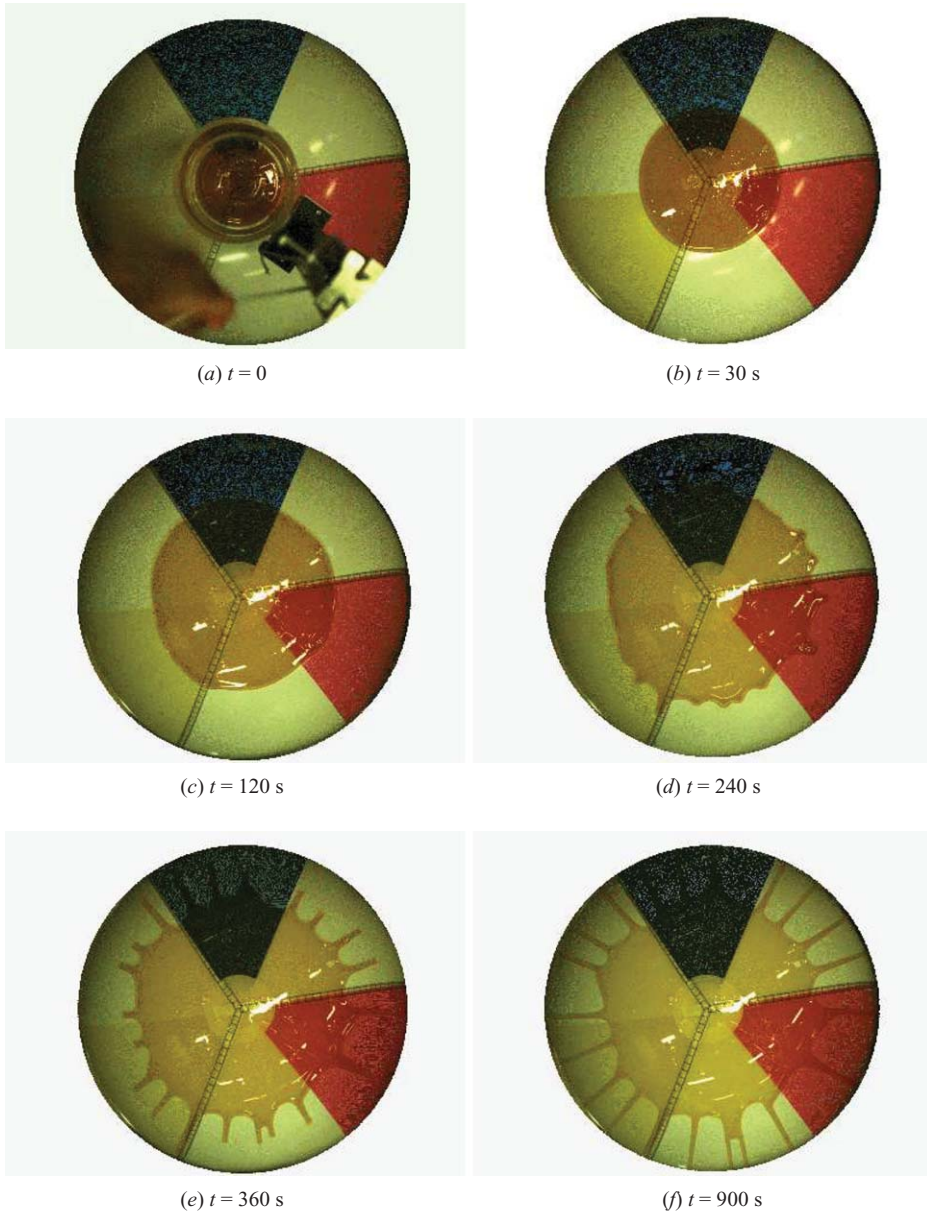


FIGURE 5. Sequence of snapshots taken from above a six-sector beach ball of radius  $R = 23$  cm, on which  $123 \text{ cm}^3$  of golden syrup was released. (a) Golden syrup is released by rapidly lifting a cylindrical gate. (b) 30 s later, the structure of the flow continues to take a circular plan form. (c) 120 s after release, the flow remains approximately axisymmetric. (d) 240 s after release, wave patterns begin to develop at the leading edge of the flow. (e) 360 s after release, the amplitude of the instability at the flow front grows and develops a series of rivulets. (f) 900 s after release, the rivulets continue to flow down the beach ball, eventually detaching from the underside (not shown). The experimental parameters are kinematic viscosity  $\nu = 4.5 \times 10^2 \text{ cm}^2 \text{ s}^{-1}$  and surface tension  $\gamma = 78 \text{ mN m}^{-1}$  (Llewellyn, Mader & Wilson 2002).

play a minor role. For example, the viscosity of fluid appears only to set the time scale and not the length scale of the flow resulting from the release of a constant volume of fluid (Huppert 1982). Experiments suggest that effects due to the contact angle

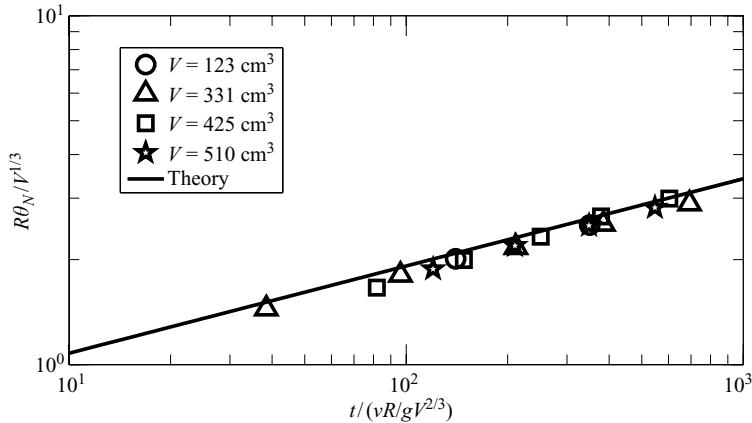


FIGURE 6. Non-dimensionalized average flow lengths against non-dimensional time on the top of a sphere before rivulets developed. Different symbols correspond to experiments conducted by releasing different volumes of golden syrup. The black line is the theoretical relationship given by (3.7).

at the flow front do not influence the onset of the instability either (Silvi & Dussan 1985). Conjecturing that the onset of the instability is determined by the length scale  $l$  of the small capillary region near the flow front, we develop dimensional arguments to suggest scalings of the flow at the onset. The two important limits of small and large Bond numbers will be treated separately, using ideas that have been developed in the well-studied context of flow down an inclined plane.

In the limit of small Bond numbers, surface tension initially plays a role not only at the tip of the current but also in the bulk region of the flow. It has been proposed that the bulk structure of the flow is stable until the flow extends a distance  $x_c \sim l$  (Troian *et al.* 1989). The current at the onset of the instability must extend sufficiently to develop a capillary ridge near the flow front ahead of a region where gravity dominates. Numerical simulations of a thin film flowing down an inclined plane (Schwartz 1989) support the idea that gravity drives the fingering instability with a characteristic wavelength set by surface tension. The condition that gravity dominates in the bulk flow at the onset of the instability suggests that the critical distance  $x_c$ , scaled by the length scale of the bulk flow, increases in the limit of small Bond numbers.

In the limit of large Bond numbers, surface tension is initially negligible everywhere, including the region near the flow front. The flow front features a recirculating nose, which has been shown experimentally to extend initially without any development of a fingering instability (Ancy, Cochard & Andreini 2009). The apparent contact angle of the advancing front is initially obtuse because gravity pushes the nose farther than the contact line. It has been suggested that the fingering instability develops when the contact angle and the capillary number of the flow front have decreased sufficiently (Veretennikov, Indeikina & Chang 1998). Effects due to surface tension begin to play a role at the tip of the current when its thickness decreases and approaches the capillary length scale,  $l_c$ . We therefore conjecture that  $h_N \sim l_c$  at the onset of the fingering instability of a current initially unaffected by surface tension everywhere. The condition that the length scale of the tip of the current must decrease to its capillary length scale before the front splits into rivulets suggests that the critical distance  $x_c$ , scaled by the length scale of the bulk flow, increases again in the limit of large Bond numbers.

The ideas developed above can be applied to the flow and instability of thin films on a cylinder and sphere. By balancing the magnitude of the bulk flow length in (2.15) with the capillary length scale of the front in (2.18) and coupling the result with (2.17), we obtain the length of the current on a cylinder for small Bond numbers at the onset of the instability:

$$x_c \sim A^{1/2} Bo^{-1/5}. \quad (5.1)$$

The critical length increases in the limit of small Bond numbers, as expected. By balancing the magnitude of the flow thickness in (2.17) with the capillary length scale of the front in (2.18), we obtain the length of the current on a cylinder for large Bond numbers at onset,

$$x_c \sim A^{1/2} Bo. \quad (5.2)$$

This indicates that the critical length increases in the limit of large Bond numbers. Note that  $x_c$  is a monotonically increasing function of  $A$  for all Bond numbers. Corresponding results are obtained for the length of the current at the onset of instability on a sphere,

$$x_c/V^{1/3} \sim \begin{cases} Bo_V^{-1/6}, & \text{small } Bo_V, \\ Bo_V^{1/3}, & \text{large } Bo_V. \end{cases} \quad (5.3)$$

The critical length at the onset is a monotonically increasing function of the volume of fluid,  $V$ . For fixed  $V$ , the critical length increases in the limits of both small and large Bond numbers.

Given that the dimensionless length of the current at the onset of the instability increases in the limits of both small and large Bond numbers, there must be an intermediate range of Bond numbers where the dimensionless length is minimal. This is consistent with the dimensionless radius of a spinning drop at the onset of the fingering instability, which is minimal for Bond numbers  $\rho\omega^2V/\gamma \sim 50$  (Wang & Chou 2001). Figure 5 of Wang & Chou (2001) shows that the dimensionless radius of spinning drops at the onset depends weakly on the Bond number, when it is neither too small or large.

Our experiments on both the cylinder and the sphere were conducted over an intermediate range of Bond numbers. Consequently, the length of the current at the onset of the instability is expected to depend weakly on the Bond number. This is consistent with figure 4, which shows that rivulets on a cylinder developed when the flow front advanced  $\simeq 8A^{1/2}$  in experiments, independent of the Bond number. Figure 7 plots the mean radius of flows spreading on a sphere at the onset of the fingering instability, as a function of the Bond number given by (3.9). The critical length of the flow increases slowly and depends weakly on the Bond number. A least-square fit to the data yields  $x_c/V \simeq 1.4Bo_V^{0.13}$  within an intermediate range of Bond numbers, consistent with scalings for small and large Bond numbers given in (5.3).

The wavelength of the fingering instability was estimated by dividing the circumference of the plan form at the onset of the instability by the number of rivulets observed subsequently. The dimensionless wavelength is plotted against the Bond number  $Bo_V$  on logarithmic scales in figure 8. The line of best fit shown in figure 8 scales like  $Bo_V^{-0.52}$  and indicates that the dimensionless wavelength decreases with Bond number. Conjecturing that the wavelength is set by the length scale of the

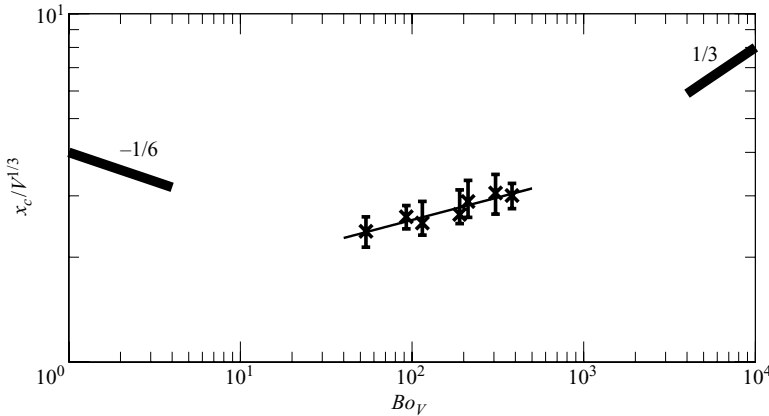


FIGURE 7. Log–log plot of the lengths of golden syrup spreading on a sphere at the onset of the fingering instability against the Bond number given by (3.9), where representative values of  $\rho = 1.4 \text{ kg m}^{-3}$ ,  $g = 9.8 \text{ m s}^{-2}$ ,  $\gamma = 78 \text{ mN m}^{-1}$  and  $R = 0.24 \text{ m}$  were fixed. The Bond number was varied in different runs by releasing different volumes of fluid. The average flow lengths at the onset of instability are represented by crosses with associated error bars indicating the maximum and minimum flow lengths for each experiment. The line of best fit through the experimental data has a slope of 0.13, which lies between the two limits of  $-1/6$  and  $1/3$  as predicted by (5.3) for small and large Bond numbers.

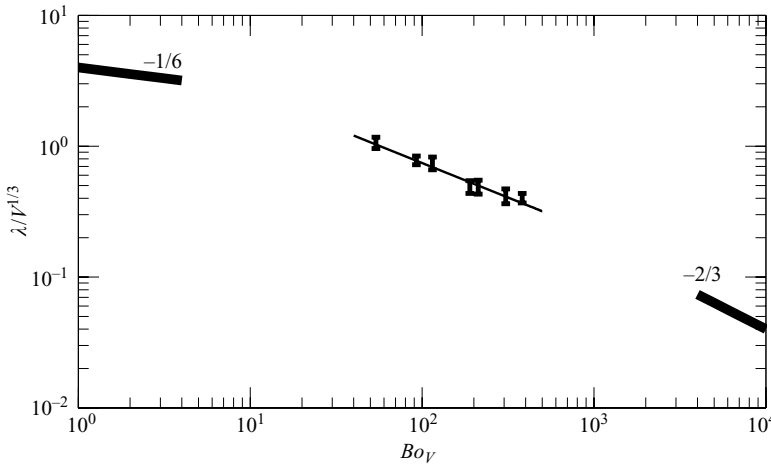


FIGURE 8. Wavelengths of the fingering instability of golden syrup spreading on a sphere as a function of the Bond number given by (3.9), where  $\rho = 1.4 \text{ kg m}^{-3}$ ,  $g = 9.8 \text{ m s}^{-2}$ ,  $\gamma = 78 \text{ mN m}^{-1}$  and  $R = 0.24 \text{ m}$ . Wavelengths were estimated by dividing the circumference of the leading edge of the flow at the onset of instability by the number of rivulets observed subsequently. Error bars are associated with the maximum and minimum flow lengths recorded at the onset of the instability for each experiment. The line fitting the average wavelengths has a gradient of  $-0.52$ , which lies between the two limits of  $-2/3$  and  $-1/6$  as predicted in (5.4) for large and small Bond numbers.

tip of the current  $l$  in (2.18) (Huppert 1982), the wavelength scales like

$$\lambda/V^{1/3} \sim \begin{cases} Bo_V^{-1/6}, & \text{small } Bo_V, \\ Bo_V^{-2/3}, & \text{large } Bo_V. \end{cases} \quad (5.4)$$

The exponent of  $-0.52$  obtained from the experiments for an intermediate range of Bond numbers lies between the limiting exponents of  $-1/6$  and  $-2/3$  for small and large Bond numbers, respectively.

The number of rivulets produced at the top of a sphere is given by

$$N = 2\pi x_c / \lambda, \quad (5.5)$$

when a sufficiently small volume of fluid is released such that  $x_c \ll R$ . By substituting (5.3) and (5.4) into (5.5), we estimate the number of rivulets to remain constant, or increase linearly with Bond number, in the limits of small and large Bond numbers, respectively. This is consistent with the trend of the number of fingers produced on a rotating plane shown in figure 12 of Wang & Chou (2001). Rivulets are not expected to develop on a cylinder or sphere when a sufficiently large volume of fluid is released.

## 6. Concluding remarks

We conclude that thin films spreading at the top of a cylinder and sphere result in a succession of events. Initially, flows on both the cylinder and sphere evolve with uniform thickness. The leading edge of the flows, after extending a critical distance, splits into a series of rivulets. The critical distance was shown experimentally to depend primarily on the volume of fluid released, for Bond numbers that are not too small or large. The relevant length scale is set by either the square root of the cross-sectional area of fluid or the cube root of the volume released for two-dimensional or axisymmetric spreading, respectively. Experiments further showed that the rivulets extend along the cylinder and sphere until they eventually detach and develop pendent threads.

The detachment of fluid before it has reached the bottom of the cylinder or sphere gives rise to an interesting problem. Experiments reported in §4 showed that releasing a relatively small volume of fluid at the top of the cylinder and sphere does not result in complete coating of the cylinder or sphere. We conducted further experiments and observed that releasing a relatively large volume of fluid at the top of a cylinder does not result in complete coating either. Approximately  $300 \text{ cm}^3$  of golden syrup, poured from a beaker immediately above a cylindrical rod of steel of diameter 1.2 cm with its axis pointing horizontally, left a small uncoated region along the bottom of the rod. This qualitative observation indicates that it is difficult to completely coat the outer surface of a cylinder or sphere by releasing fluid from above.

A complete coating of the outer surfaces of a cylinder and sphere could be obtained instead by dipping them into and withdrawing from a bath of viscous fluid, a familiar method in coating industries. Thin films are expected to develop and drain as investigated in §§2 and 3 near the top of the cylinder and sphere. In contrast to a film of fluid draining from a vertical plate, which is always thicker towards the bottom of the plate (Jeffreys 1931), the thickness of fluid draining from the top of the cylinder and sphere should remain uniform.

We are pleased to submit this work on thin films, one of the many research interests of Steve Davis, in honour of his seventieth birthday. One of us (H. E. H.) has known, admired and learnt from Steve since we first met at a seminar at Woods Hole during the summer of 1973. The speaker stated a fluid mechanical concept; a member of the audience enquired why it was correct; and the speaker replied: it appeared recently

in *JFM*—so it must be correct. Steve and H. E. H., both assistant editors of *JFM* at the time, smiled.

We thank Mark Hallworth and David Page-Croft for their assistance with the experimental set-ups. We also thank John Hinch, Richard Katz, John Lister, Jerome Neufeld and Howard Stone for helpful and insightful ideas. Mark Hallworth and Jerome Neufeld provided useful comments on an earlier draft. D. T. is funded by a Gates Cambridge Scholarship. The research of H. E. H. is partially supported by a Royal Society Wolfson Research Merit Award. Draft versions of the manuscript were completed while one of us (H. E. H.) worked at the desk of the Chancellor of the University of New South Wales, David Gonski. H. E. H. is grateful for the generous hospitality shown by the Chancellor and all the staff during his visit.

## REFERENCES

- ACHESON, D. J. 1990 *Elementary Fluid Dynamics*. Oxford University Press.
- ANCEY, C., COCHARD, S. & ANDREINI, N. 2009 The dam-break problem for viscous fluids in the high-capillary-number limit. *J. Fluid Mech.* **624**, 1–22.
- BERTOZZI, A. L. & BRENNER, M. P. 1997 Linear stability and transient growth in driven contact lines. *Phys. Fluids* **9**, 530.
- CAZABAT, A. M., HESLOT, F., TROIAN, S. M. & CARLES, P. 1990 Fingering instability of thin spreading films driven by temperature gradients. *Nature* **346** (6287), 824–826.
- DAVIS, S. H. 1983 Contact-line problems in fluid mechanics. *J. Appl. Mech.* **50** (4B), 977–982.
- DUFFY, B. R. & MOFFATT, H. K. 1995 Flow of a viscous trickle on a slowly varying incline. *Chem. Engng J. Biochem. Engng J.* **60** (1–3), 141–146.
- FRAYSSE, N. & HOMSY, G. M. 1994 An experimental study of rivulet instabilities in centrifugal spin coating of viscous Newtonian and non-Newtonian fluids. *Phys. Fluids* **6**, 1491.
- GOODWIN, R. & HOMSY, G. M. 1991 Viscous flow down a slope in the vicinity of a contact line. *Phys. Fluids A: Fluid Dyn.* **3**, 515.
- HUPPERT, H. E. 1982 Flow and instability of a viscous current down a slope. *Nature* **300** (5891), 427–429.
- INDEIKINA, A., VERETENNIKOV, I. & CHANG, H. C. 1997 Drop fall-off from pendent rivulets. *J. Fluid Mech.* **338**, 173–201.
- JEFFREYS, H. 1931 The drainage of a vertical plate. *Proc. Cambridge Philos. Soc.* **26**, 204–205.
- LLEWELLIN, E. W., MADER, H. M. & WILSON, S. D. R. 2002 The rheology of a bubbly liquid. *Proc. R. Soc. Math. Phys. Engng Sci.* **458** (2020), 987–1016.
- MELO, F., JOANNY, J. F. & FAUVE, S. 1989 Fingering instability of spinning drops. *Phys. Rev. Lett.* **63** (18), 1958.
- MOFFATT, H. K. 1977 Behaviour of a viscous film on the outer surface of a rotating cylinder. *J. de Mécanique* **16** (5), 651–673.
- ORON, A., DAVIS, S. H. & BANKOFF, S. G. 1997 Long-scale evolution of thin liquid films. *Rev. Mod. Phys.* **69** (3), 931–980.
- ROTHROCK, D. A. 1968 Study of flows down the underside of an inclined plane. PhD thesis, University of Cambridge.
- ROY, R. V., ROBERTS, A. J. & SIMPSON, M. E. 2002 A lubrication model of coating flows over a curved substrate in space. *J. Fluid Mech.* **454**, 235–261.
- SCHWARTZ, L. W. 1989 Viscous flows down an inclined plane: instability and finger formation. *Phys. Fluids A: Fluid Dyn.* **1**, 443.
- SHORT, M. B., BAYGENTS, J. C., BECK, J. W., STONE, D. A., TOOMEY, R. S. & GOLDSTEIN, R. E. 2005 Stalactite growth as a free-boundary problem: a geometric law and its platonic ideal. *Phys. Rev. Lett.* **94** (1), 18501.
- SILVI, N. & DUSSAN, E. B. V. 1985 On the rewetting of an inclined solid surface by a liquid. *Phys. Fluids* **28** (1), 5–7.
- SPAID, M. A. & HOMSY, G. M. 1996 Stability of Newtonian and viscoelastic dynamic contact lines. *Phys. Fluids* **8**, 460.

- STONE, H. A. 2005 On lubrication flows in geometries with zero local curvature. *Chem. Engng Sci.* **60** (17), 4838–4845.
- TROIAN, S. M., HERBOLZHEIMER, E., SAFRAN, S. & JOANNY, J. F. 1989 Fingering instabilities of driven spreading films. *Europhys. Lett.* **10**, 25–30.
- VERETENNIKOV, I., INDEIKINA, A. & CHANG, H. C. 1998 Front dynamics and fingering of a driven contact line. *J. Fluid Mech.* **373**, 81–110.
- WANG, M. W. & CHOU, F. C. 2001 Fingering instability and maximum radius at high rotational bond number. *J. Electrochem. Soc.* **148**, G283.